

Supplementary Information for Dynamic Hovering for Uncrewed Underwater Vehicles via An Error-Separation-based Cooperative Strategy

Xiaoli Luan¹, Shenhan Yu¹, and Haiying Wan^{1,*}

¹the Key Laboratory of Advanced Control for Light Industry Processes. Ministry of Education, Jiangnan University, Wuxi 214122, China

*whywan@jiangnan.edu.cn

ABSTRACT

Performance comparison under increasing current disturbance

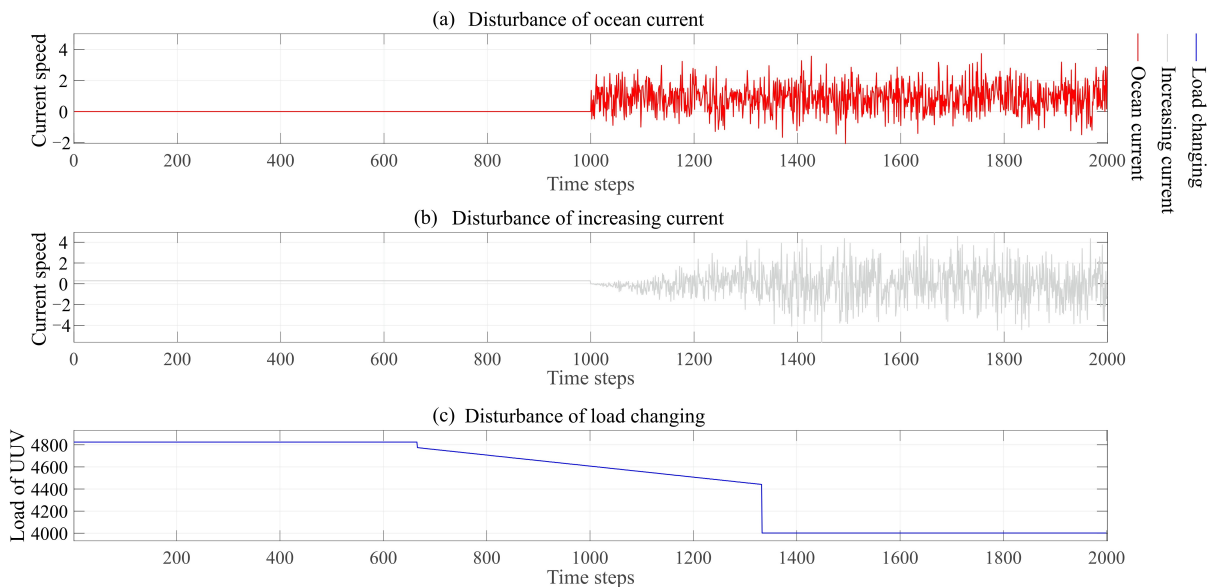


Figure 1. Disturbances of ocean current, increasing current and load changing. Subfigure (a) presents the ocean current disturbance, while Subfigure (b) illustrates the scenario in which the UUV is influenced by an increasing current disturbance. Meanwhile, Subfigure (c) depicts the disturbance caused by load changes.

Different types and levels of disturbances exert varying impacts on the control performance of UUVs. This section examines the robustness of the proposed control scheme in handling other scenarios including ocean current disturbance, increasing current disturbance and load changing disturbance. As depicted in Figure 1 (a), ocean current is modeled as a continuous, directed flow of seawater, comprising a constant current component superimposed with Gaussian white noise. Additionally, to simulate the common phenomenon of increasing ocean current speed, a sinusoidal signal with gradually rising amplitude, combined with Gaussian white noise, is employed, as shown in Figure 1 (b). Beyond ocean current disturbance, UUVs frequently encounter load variations during deep-sea missions, such as towing, collecting, and releasing operations, which alter their kinetic properties and thrust-to-acceleration dynamics. To evaluate the impact of load changes, a general load variation scenario is simulated in Figure 1 (c). This involves a continuous load reduction from steps 600 to 1300, followed by an abrupt load jump after step 1300, effectively capturing the dynamic load conditions experienced by UUVs in real-world applications.

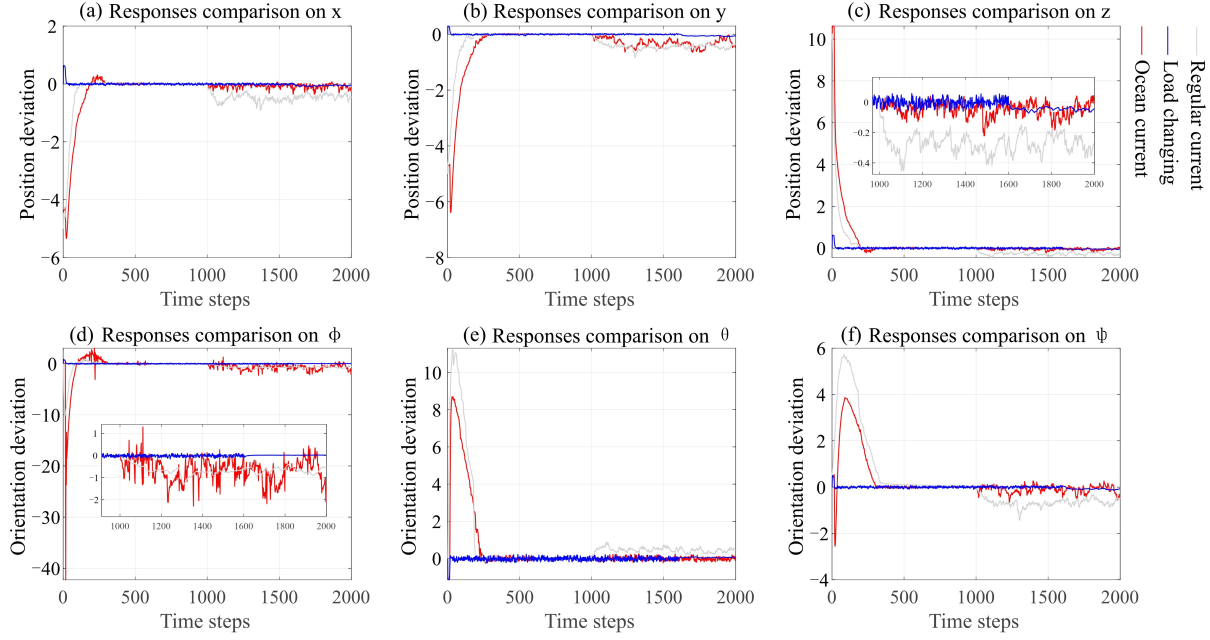


Figure 2. State responses of UUV under the control of COC influenced by different disturbances. Subfigure (a) illustrates the state response of position x , while Subfigures (b) and (c) depict the state responses of positions y and z , respectively. Similarly, Subfigures (d), (e), and (f) present the state responses of orientation ϕ , θ , and ψ , respectively. The red, blue, and gray lines correspond to the state responses of COC under ocean current conditions, load-changing scenarios, and regular current conditions.

For the ocean current scenario, as shown in Figure 2, the trend closely follows that of the gray lines. It indicates that the pose deviations under ocean current influence are smaller compared to those caused by current disturbances. This suggests that the proposed COC framework effectively mitigates the impact of ocean currents better than in the regular case. In the load-changing scenario depicted in Figure 2, the overshoot remains minimal, the trends of state response curve are smooth, and the steady-state error is negligible. These characteristics demonstrate that under COC control, variations in the UUV's load exert minimal influence on system performance. Consequently, there is no necessity to redesign the controller parameters in response to the UUV's load changing case.

Figure 3 depicts the state responses of systems controlled by LQR, SMC, and COC (in blue, red, and gray lines, respectively) under increasing current conditions. Notably, the red lines exhibit violent oscillations and divergent trends in sub-figures (a) and (b), while converging in others. This suggests that when ocean currents surpass the SMC's acceptable upper limit, the system becomes unstable. In contrast, the COC oscillate but converge, closely tracking the blue lines, indicating that COC mitigates the divergent trend in SMC. This resilience stems from COC's collaborative mechanism, which addresses system divergence caused by single controller failure. In this framework, even if SMC diverges, COC's thrust is constrained by the LQR component, preventing worst-case scenarios. In summary, this subsection demonstrates the effectiveness of the developed COC approach in managing ocean currents, load changes, and increasing currents. Even when sub-controllers fail to stabilize the system, COC avoids critical failures, thereby enhancing the UUV's robustness.

Figure 3 illustrates the state responses of systems controlled by LQR, SMC, and COC under increasing current conditions. Notably, in subfigures (a) and (b), the responses of SMC exhibit severe oscillations and a divergent trend, whereas they converge in the remaining subfigures. This indicates that when ocean currents exceed SMC's robust limits, the system becomes unstable. In contrast, although COC exhibits oscillatory behavior, it ultimately converges and closely follows the blue lines. This demonstrates its ability to suppress SMC's divergence. This robustness arises from COC's collaborative mechanism, which compensates for instability resulting from the failure of a single controller. Specifically, even if SMC diverges, COC constrains thrust through its LQR component, preventing worst-case instability.

In summary, this analysis highlights the effectiveness of the proposed COC approach in handling ocean currents, load variations, and increasing current disturbances. Even when individual sub-controllers fail to maintain system stability, COC prevents severe instability, thereby significantly enhancing the robustness of the UUV.

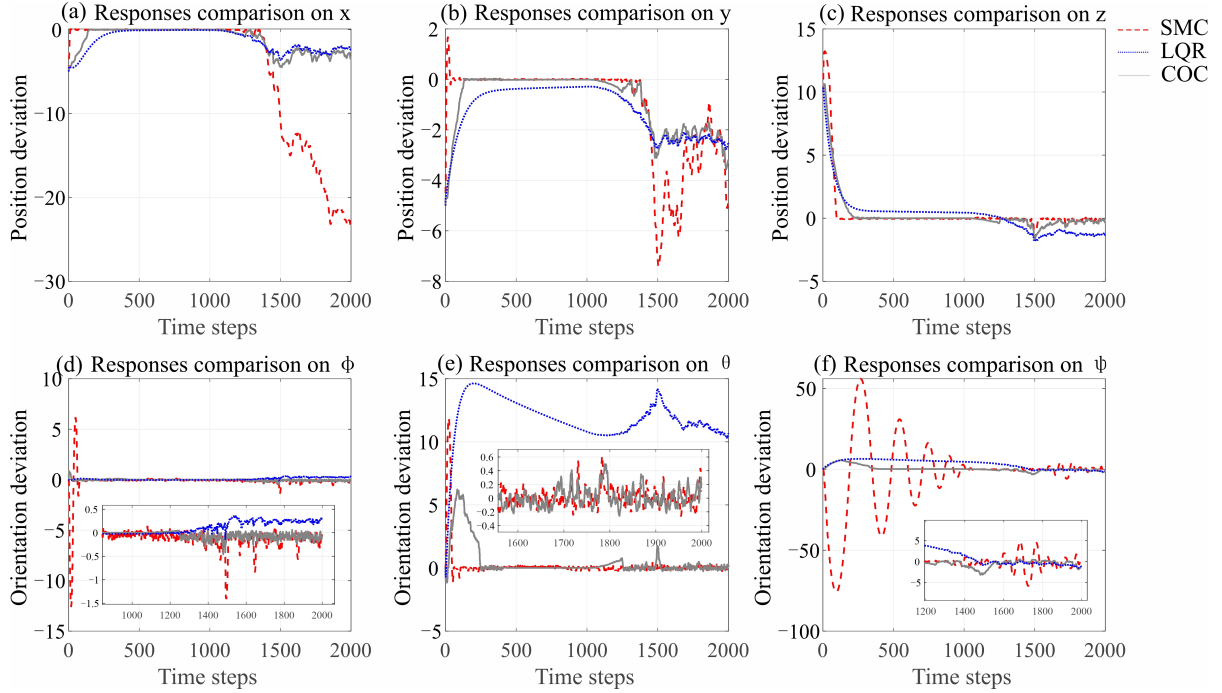


Figure 3. State responses of UUV under different controllers influenced by increasing current. Subfigure (a) depicts the state response for the positional coordinate x , while (b) illustrates the response for y , and (c) presents the response for z . Regarding the orientation, (d) shows the state response for ϕ , (e) displays the response for θ , and (f) outlines the response for ψ . The red, blue, and gray lines represent the LQR, SMC, and COC control strategies, respectively.

Preliminary knowledge of SMC (Sliding mode Control)

Consider a discrete UUV system in the form of:

$$\begin{cases} \mathbf{v}_{k+1} = -\{\mathbf{M}(\mathbf{v}_k)^{-1}[\mathbf{C}(\mathbf{v}_k)\mathbf{v}_k + \mathbf{D}(\mathbf{v}_k)\mathbf{v}_k + \mathbf{g}(\eta_k)] + \mathbf{M}(\mathbf{v}_k)^{-1}(\tau_{\delta,k} + \delta_k)\}dt + \mathbf{v}_k, \\ \eta_{k+1} = [\mathbf{J}(\eta_k)\mathbf{v}_k]dt + \eta_k, \end{cases} \quad (1)$$

where the terms have the same meaning as defined in the paper. For clarity, we restate these definitions in Remark 1.

Remark 1 *dt represents the sampling time, determined by the hardware requirements, and k denotes the discrete time index. \mathbf{v}_k , \mathbf{v}_{k+1} , and η_k , η_{k+1} represent the velocity vector \mathbf{v} and the orientation vector η at time steps k and $k+1$, respectively. $\tau_{\delta,k}$ and δ_k denote the control input and the current disturbance at time step k. The matrices $\mathbf{M}(\mathbf{v}_k)$, $\mathbf{C}(\mathbf{v}_k)$, $\mathbf{D}(\mathbf{v}_k)$, $\mathbf{g}(\eta_k)$, and $\mathbf{J}(\mathbf{v}_k)$ represent the corresponding functions of \mathbf{v}_k and η_k in the discrete-time model.*

Due to the influence of changes in the orientation and velocity of the UUV on system matrices like $\mathbf{M}(\mathbf{v}_k)$, coupled with the current disturbance, the system exhibits strong nonlinear characteristics and is highly disturbed. This can lead to the failure of certain control strategies to stabilize the system. To achieve good control accuracy with the nonlinear model under the influence of disturbance δ_k , we first apply a sliding mode control strategy to stabilize the UUV model.

Design the following sliding surface constraining both position deviation and speed deviation:

$$\mathbf{s}_{\delta,k} = \mathbf{c}\mathbf{v}_{\delta,k} + \eta_{\delta,k}, \quad (2)$$

where \mathbf{s}_k is the weight to balance whether to focus more on the deviation on position or speed. With a sign function $\dot{\mathbf{s}} = -\rho \text{sgn}(\mathbf{s})$ play as the reaching law of SMC, and formulate its discrete form:

$$\frac{\mathbf{s}_{\delta,k+1} - \mathbf{s}_{\delta,k}}{dt} = -\rho \text{sgn}(\mathbf{s}_{\delta,k}). \quad (3)$$

Substitute the discrete model information and 2 into equation 3 and simplify them, we can get:

$$\tau_{\delta,k} = \mathbf{C}(\mathbf{v}_k)\mathbf{v}_{\delta,k} + \mathbf{D}(\mathbf{v}_k)\mathbf{v}_{\delta,k} + \mathbf{g}(\eta_k) - \mathbf{M}(\mathbf{v}_k)\mathbf{c}^{-1}\mathbf{J}\mathbf{v}_{\delta,k} - \mathbf{M}\mathbf{c}^{-1}\rho \text{sgn}(\mathbf{s}_{\delta,k}). \quad (4)$$

Thus, the sliding mode control law for the UUV is derived. Under this control strategy, the sliding mode state will eventually converge to the vicinity of the sliding mode surface $s_{\delta,k} = 0$ within a boundary Δ and remain there indefinitely¹. Specifically, $|s_{\delta,k}| \leq \Delta$ for all $k > k^*$, where k^* is a constant. To determine the specific value of Δ , we substitute 4 and 3 into the UUV model and simplify the resulting expression:

$$s_{\delta,k+1} = s_{\delta,k} - \rho sgn(s_{\delta,k})dt + cM(v_k)^{-1}\delta_k dt. \quad (5)$$

As $s_{\delta,k}$ eventually approaches zero, the bias between $s_{\delta,k}$ and $s_{\delta,k+1}$ arises from the disturbance δ_k and the thrust $\tau_{\delta,k}$, which compensates for the previous disturbance δ_{k-1} . Therefore, it can be concluded that once the conditions mentioned above are met, the sliding mode surface $s_{\delta,k}$ will be bounded within Δ , where $\Delta = \rho sgn(s_{\delta,k}) + cM^{-1}\delta_k dt$. This ensures that the system will remain stable.

Preliminary knowledge of LQR (Linear Quartic Optimal Control)

As formulates in the paper, the linear discrete model of the UUV's hoving task has been obtained as:

$$\mathbf{x}_{k+1} = \mathbf{A}_k \mathbf{x}_k + \mathbf{B}_k \tau_k + \delta_k + \mathbf{w}_k, \quad (6)$$

where the terms have the same meaning as those in the paper. For ease of understanding, we reproduce the expression for the system matrix \mathbf{A}_k , the input matrix \mathbf{B}_k , and other definitions in Remark 2.

$$\begin{aligned} \mathbf{A}_k &= \begin{bmatrix} (\frac{\partial \mathbf{J}(\eta_0) v_0}{\partial \eta_0} + \mathbf{I})dt \\ -\frac{\partial \mathbf{M}(v_0)^{-1} \mathbf{g}(\eta_0)}{\partial \eta_0} dt & [\mathbf{I} - \frac{\partial \mathbf{H}(v_0, \tau_0)}{\partial v_0}]dt \end{bmatrix}, \mathbf{B}_k = \begin{bmatrix} 0 & \frac{\partial \mathbf{M}(v_0)^{-1} \tau_0}{\partial \tau_0} dt \end{bmatrix}^T, \\ \mathbf{H}(v_0, \tau_0) &= \mathbf{M}(v_0)^{-1} \mathbf{C}(v_0) v_0 + \mathbf{M}(v_0)^{-1} \mathbf{D}(v_0) v_0 + \mathbf{M}(v_0)^{-1} \mathbf{g}(\eta_0) - \mathbf{M}(v_0)^{-1} \tau_0. \end{aligned} \quad (7)$$

Remark 2 η_0 , v_0 , and τ_0 represent the values of η , v , and τ^δ at the time step $k = 0$, respectively. \mathbf{I} is the identity matrix with the same dimensions as $\mathbf{J}(\eta_k)$. $\mathbf{H}(v_0, \tau_0)$ is an intermediate variable introduced to simplify the notation. \mathbf{x}_k and τ_k represent the system state and thrust input of the mismatched model, respectively. Their physical meanings are identical to those of \mathbf{x}_k^δ and $\tau_{\delta,k}$. The only distinction is that, in contrast to model (1), random noise \mathbf{w}_k from the thrusters is introduced. The remaining terms are consistent with those in model (1).

The former strategy, SMC, tends to provide high-gain input with high-frequency oscillations, which is known as "chattering". This can cause excessive wear and tear on actuators and degrade the performance of the control system while increasing the control consumption. To reach the balance between control accuracy and consumption, a H_2 controller is designed to carry out the task. But since it works for system without disturbance, we need to first simplify the UUV model as:

$$\mathbf{x}_{\epsilon,k+1} = \mathbf{A}_k \mathbf{x}_{\epsilon,k} + \mathbf{B}_k \tau_{\epsilon,k} + \mathbf{w}_k, \quad (8)$$

where $\mathbf{x}_{\epsilon,k}$ and $\tau_{\epsilon,k}$ stand for the deviation state and thrust when the system is not influenced by current disturbance. The rest terms remain the same as the actual model 6.

$$\begin{cases} J_k^* = \min_{\tau_k} \left[(\mathbf{x}_{\epsilon,k}^T \mathbf{Q} \mathbf{x}_{\epsilon,k} + \tau_k^T \mathbf{R} \tau_k) + \mathbf{x}_{k+1}^T \mathbf{P}_{k+1} \mathbf{x}_{k+1} \right], \\ \tau_k^* = \min_{\tau_k} \{ J_k + [\mathbf{x}_{k+1}^T \mathbf{P}_{k+1} \mathbf{x}_{k+1} - \mathbf{x}_{\epsilon,k+1}^T \mathbf{P}_{k+1} \mathbf{x}_{\epsilon,k+1}] \}. \end{cases} \quad (9)$$

$$J_k = \mathbf{x}_{k+1}^T \mathbf{P}_{k+1} \mathbf{x}_{k+1}, J_{\epsilon,k} = \mathbf{x}_{\epsilon,k+1}^T \mathbf{P}_{k+1} \mathbf{x}_{\epsilon,k+1}, \quad (10)$$

Define the cost function as $F = \mathbf{x}_k^T \mathbf{Q} \mathbf{x}_k + \tau_k^T \mathbf{R} \tau_k$, and solve a QP(Convex Quadratic Programming) problem using the Riccati equation². We can get the feedback control law as:

$$\tau_k^* = -\mathbf{K}_\epsilon \mathbf{x}_k, \quad (11)$$

$$\mathbf{K}_\epsilon = -(\mathbf{R} + \mathbf{B}_k^T \mathbf{P}_{k+1} \mathbf{B}_k)^{-1} \mathbf{B}_k^T \mathbf{P}_{k+1} \mathbf{A}_k, \quad (12)$$

where \mathbf{K}_ϵ is the optimal control gain and \mathbf{P}_k satisfies a discrete algebra Riccati equation (ARE)

$$\mathbf{P}_{k+1} = \mathbf{A}_k^T \mathbf{P}_k \mathbf{A}_k - \mathbf{A}_k^T \mathbf{P}_k \mathbf{B}_k (\mathbf{R} + \mathbf{B}_k^T \mathbf{P}_k \mathbf{B}_k)^{-1} \mathbf{B}_k^T \mathbf{P}_k \mathbf{A}_k + \mathbf{Q} \quad (13)$$

References

1. Ma, H., Wu, J. & Xiong, Z. Discrete-time sliding-mode control with improved quasi-sliding-mode domain. *IEEE Transactions on Ind. Electron.* **63**, 6292–6304 (2016).
2. Tijjani, A. S., Chemori, A. & Creuze, V. A survey on tracking control of unmanned underwater vehicles: Experiments-based approach. *Annu. Rev. Control.* **54**, 125–147 (2022).